HAL
open science

Tractography via the Ensemble Average Propagator in diffusion MRI

Sylvain Merlet, Anne-Charlotte Philippe, Rachid Deriche, Maxime Descoteaux

To cite this version:

Sylvain Merlet, Anne-Charlotte Philippe, Rachid Deriche, Maxime Descoteaux. Tractography via the Ensemble Average Propagator in diffusion MRI. Medical Image Computing and Computer Assisted Intervention (MICCAI), Oct 2012, Nice, France. pp.7511. hal-00727797

HAL Id: hal-00727797

https://hal.science/hal-00727797v1

Submitted on 4 Sep 2012

HAL is a multi-disciplinary open access archive for the deposit and dissemination of scientific research documents, whether they are published or not. The documents may come from teaching and research institutions in France or abroad, or from public or private research centers.

L'archive ouverte pluridisciplinaire **HAL**, est destinée au dépôt et à la diffusion de documents scientifiques de niveau recherche, publiés ou non, émanant des établissements d'enseignement et de recherche français ou étrangers, des laboratoires publics ou privés.

Tractography via the Ensemble Average Propagator in diffusion MRI

Sylvain Merlet[1], Anne-Charlotte Philippe[1], Rachid Deriche[1], Maxime Descoteaux[2]

[1] Athena Project-Team, INRIA Sophia Antipolis - Méditerranée, France
[2] Sherbrooke Connectivity Imaging Laboratory (SCIL), Canada

Abstract. It's well known that in diffusion MRI (dMRI), fibre crossing is an important problem for most existing diffusion tensor imaging (DTI) based tractography algorithms. To overcome these limitations, High Angular Resolution Diffusion Imaging (HARDI) based tractography has been proposed with a particular emphasis on the the Orientation Distribution Function (ODF). In this paper, we advocate the use of the Ensemble Average Propagator (EAP) instead of the ODF for tractography in dMRI and propose an original and efficient EAP-based tractography algorithm that outperforms the classical ODF-based tractography, in particular, in the regions that contain complex fibre crossing configurations. Various experimental results including synthetic, phantom and real data illustrate the potential of the approach and clearly show that our method is especially efficient to handle regions where fiber bundles are crossing, and still well handle other fiber bundle configurations such as U-shape and kissing fibers.

1 Introduction

At the current resolution of diffusion-weighted (DW) magnetic resonance imaging (MRI), research groups agree that there are between one and two thirds of imaging voxels in the human brain white matter that contain fibre crossing bundles [8]. We know that in these locations, the diffusion is non-Gaussian and the diffusion tensor (DT) [3] is limited due to its intrinsic Gaussian diffusion assumption. Hence, DT-based tractography algorithms can follow false tracts and produce unreliable tracking results. To overcome limitations of the DT, new HARDI techniques have been proposed to estimate the diffusion orientation distribution function (ODF) [10, 5, 1, 9] of water molecules. These HARDI techniques were developed to deal with non-Gaussian diffusion processes and because the maxima of the ODF are aligned with the underlying fibre populations, deterministic and probabilistic ODF-based tractography algorithms have been proposed [5] that outperform classical DT-based tractography algorithms. In this paper, we mainly advocate the use of the Ensemble Average Propagator (EAP) instead of the ODF for tractography in dMRI and propose an original and efficient streamline EAP-based tractography algorithm that outperforms the classical ODF-based tractography, in particular in the regions that contain complex fiber crossing congurations.

2 Analytical Signal estimation and diffusion features

Recent works [2, 7, 4] propose to analytically estimate the normalized diffusion signal $E(q\mathbf{u})$ as a linear combination of 3D functions Ψ_{nlm},
$E(q\mathbf{u}) = \sum_{n=0}^{N} \sum_{l=0}^{L} \sum_{m=-l}^{l} c_{nlm} \Psi_{nlm}(q\mathbf{u})$, where q is the norm of the effective gradient, $\mathbf{u}$ a unitary vector, and n,l are respectively the radial and angular order of the associated 3D function.

In [2, 7, 4] the authors also propose analytical formulas to estimate some diffusion features. In particular, they enable to compute the EAP P at any radius R, i.e. $P(R\mathbf{r})$ with $\mathbf{r}$ a 3D unit vector. In our paper, we are especially interested in this feature. Moreover, they give analytical formulas to estimate the normalized ODF Υ expressed as the integration of the EAP over a solid angle [1, 9], $\Upsilon(\mathbf{r}) = \int_0^\infty P(R.\mathbf{r})R^2 dR$. The ODF will be used, as comparison, in order to perform the well-known ODF based streamline algorithm [5]

3 Motivations and challenges

Here, we motivate the use of the EAP instead of the ODF in order to characterize fiber orientations. Several challenges arise when dealing with the whole EAP information that must be taken into consideration. We illustrate this section by an example confronting ODF and EAP based estimation of the fiber orientations.

The ODF is known to well represent the angular structure of the diffusion phenomenon. However, it has some limitations. First, the radial integration over a solid angle is done all over the EAP, and thus is likely to catch unwanted artifact that lead to false orientation detection. The next problem arises when fiber bundles with large differences in anisotropy are crossing. We illustrate this with a synthetic data example. We consider two crossing fiber bundles, a high anisotropy fiber bundle (the curved one) and a low anisotropy fiber bundle (the diagonal one). We estimate the ODF $\Upsilon(\mathbf{r})$ and the EAP $P(R\mathbf{r})$ with radii $R = 5, 10, 15, 18\mu m$ via the SHORE method [7]. Then, we extract the maxima of each spherical function using a discrete approach. These maxima are represented by the red line. Because the diffusion in direction of the curved bundle highly predominates, we don't manage to resolve this crossing region using the ODF Υ (see Fig. 1.a). However, we see that the EAPs manage to catch some angular information where the ODFs fail. In particular, the whole crossing structure is caught at a radius $R = 18\mu m$ (see Fig. 1.e).

The EAP has also some disadvantages. Even, if it can catch more complex structure than the ODF, we need to know where the significant information is localized. Considering the EAP is near isotropic for low radii, and becomes more anisotropic for higher radii, it would be natural to consider only high EAP radii. However, this is not done for several reasons : 1) a physical reason and 2) a technical reason. First,the trajectory of water molecules can be described by a random walk, i.e. each molecule follows a random path in a 3D space. However, when looking at a set of molecules, one can see that, in a free medium, the averaged displacement follows a Gaussian distribution. It means that most of the

Fig. 1. ODF $\Upsilon(\mathbf{r})$ (a) and the EAP $P(R\mathbf{r})$ with radii $R = 5, 10, 15, 18\mu m$ (respectively b, c, d, e) estimated via the SHORE method in a synthetic crossing configuration, and extracted maximas. The curved fiber bundle has a high anisotropy and the diagonal bundle a low anisotropy.

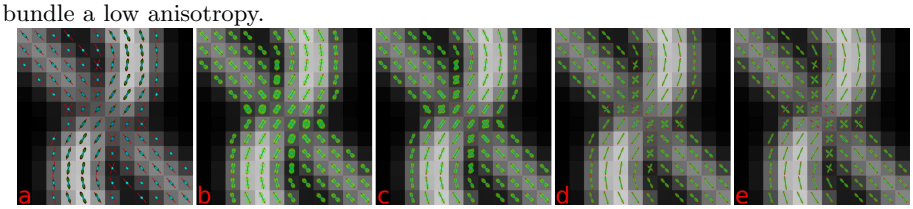

molecules remain confined around their initial positions. At the scale of a voxel, the EAP represents this averaged displacement of molecules and because of its Gaussian particular nature, the EAP values decrease while moving away from its center until falling to zero and, then, the EAP return to an isotropic state. Beside physical reasons, the maximum b-value authorized by the acquisition protocol, makes the signal band limited i.e. the high frequency component are discarded. It results in a smoothing of the EAP and a loss of details. This phenomenon emphasizes the return to an isotropic state.

Because of these two reasons, we know the significant angular information is localized away from the EAP center but not too far because of the signal decrease. Beside the difficulty to find an optimal radius, we know as well that the water molecule diffusion is likely to vary between different voxel, and the angular information we want to catch is not always localized at the same radius. Therefore, we cannot consider the EAP at only one radius for the whole tractography. Hence, the challenge is to find the optimal radius R at each voxel, on which the EAP $P(R\mathbf{r})$ optimally represents the orientation of the current fiber.

4 EAP based tractography

The main problem in recovering the fiber bundle orientations, comes from the fact that we don't know at which EAP radius R is localized the information. The challenge, as explained in section 3 is to find the optimal EAP radius R, on which we are able to catch the orientation of the current fiber.

We could proceed as follow : Starting from an initial radius, we authorize to switch to the radius R where the local maxima of $P(R\mathbf{r})$ has the largest similarity with the current fiber direction. However, if we force the fiber to find a maxima direction similar to the current fiber direction, we would take the risk to always follow the same direction (not suitable for curved fibers). This is especially true if false local maxima are detected due to noise. Our idea is to encourage the switching between close radii by inserting a penalty function, which penalizes the radii far from the current radius. It enables to obtain consistent fibers, which are more robust to noise. Then, we define the penalty function as $w_{R_c}(R)$, which measure the amount of penalty between the current radius R_c and the radius

R. We propose to use a exponential penalty function, i.e. $w_{R_c}(R) = \exp(-\beta \times \frac{|R_c - R|}{R_c})$ where β is a scale parameter.

Before continuing with the complete tracking algorithm, we need to clarify the fiber orientation detection step. Considering that we have an estimation of the EAP P, we define a procedure "ExtractAngularInformation", whose the input is $\mathbf{v}_c \in \mathbb{R}^3$ (the current fiber direction), $R_c \in \mathbb{R}$ (the current EAP radius), and $\beta \in \mathbb{R}$ (the penalty scale parameter), and returns the next direction $\mathbf{v}_n \in \mathbb{R}^3$ and the corresponding EAP radius $R_n \in \mathbb{R}$. We also need a function Extractmax(P), which return the list l_R of directions $l_R(j)$ along each maxima of $P(R\mathbf{r})$. The procedure is described in Alg. 1.

Algorithm 1 ExtractAngularInformation

Require: $\mathbf{v}_c \in \mathbb{R}^3$, $R_c \in \mathbb{R}$, $\beta \in \mathbb{R}$, the EAP P
1. Compute $w_{R_c}(R) = \exp(-\beta \times \frac{|R_c - R|}{R_c})$ for $R \in \mathbb{R}$
2. Compute l_R =extractMax(P)
3. Set $R^*, j^* = argmax_{R,j} \langle l_R(j) \cdot v_c \rangle \times w_{R_c}(R)$
4. $R_n = R^*, v_n = l_{R^*}(j^*)$

return R_n, v_n

Now we have defined a way to detect fiber orientations, we describe our deterministic tractography algorithm based on the EAP. For the purpose we extend the streamline method based on multiple ODF maxima [5]. At first, we denote p(s) as the curve parameterized by its arc-length. This curve can be computed as a 3D path adapting its tangent orientation locally according to vector field v. Hence, for a given starting point p_0, we solve $p(t) = p_0 + \int_0^t \mathbf{v}(p(s))ds$. The integration is typically performed numerically with Euler or Runge-Kutta schemes of order 2 or 4. In the Euler case, we have the discrete evolution equation $p_{n+1} = p_n + \mathbf{v}(p_n)\Delta_s$, where Δ_s is a small enough step size to obtain subvoxel precision. A continuous linear, cubic, spline interpolation of the vector field can be done at each step for the subvoxel points. For our algorithm, we need a starting seed $p_0 \in \mathbb{R}^3$, a starting radius R_0, a curvature threshold $t_\theta \in [0, 90°]$.The algorithm is described in Alg. 2. For the rest of the paper, ODF-tract refers to the ODF based streamline tractography [5], and EAP-tract refers to our EAP based tractography algorithm (Alg. 2).

5 Experiments

Synthetic data : We start by validating our method on synthetic data. For this purpose, we consider the EAP and ODF of Fig. 1. In this example, two bundles, a high anisotropy fiber bundle (the curved bundle) and a low anisotropy fiber bundle (the diagonal bundle) are crossing. Let us remind that, the EAP and ODF were estimated via the SHORE method. We first compare the EAP-tract and ODF-tract methods in case of noiseless measurements (see fig. 2 a,b). In both algorithms, we set the step $\Delta_s = 0.5$ and the curvature threshold $t_\theta = 75°$.

Algorithm 2 EAP based fibers tracking algorithm

Require: $p_0 \in \mathbb{R}^3$, $R_0 \in \mathbb{R}$, $t_{fa} \in [0,1]$, $t_\theta \in [0, 90°]$
1. Estimate field of analytical EAP estimation P
2. $\mathbf{v}_{p_0} = argmax_{\mathbf{u}}\ P_{p_0}(R_0\mathbf{u})$
3. Set $i = 0, R_i = R_0$ and **do**
   $p_{i+1} = p_i + \Delta\mathbf{v}_{p_i}$
   Update the fiber f according to p_i
   $R_{i+1}, \mathbf{v}_{p_{i+1}} = ExtractAngularInformation(\mathbf{v}_{p_i}, P_{p_i}, R_i, \beta)$
   if $\frac{\langle \mathbf{v}_{p_i} \cdot \mathbf{v}_{p_{i+1}} \rangle}{\|\mathbf{v}_{p_i}\| \|\mathbf{v}_{p_{i+1}}\|}$ **then** stop;
   $i = i + 1$
return f

The scale parameter of the penalty function in Alg. 1 is set to $\beta = 0.5$. In Fig. 2.a, we see that the diagonal fibers from the ODF-tract method fail to pass through the crossing region because the diffusion constrained by the curved fiber predominates in this area. This is not surprising while looking at Fig. 1.a, in which the ODF maxima are not sufficiently large to detect the diagonal fibers in the crossing area. However, if we look at Fig. 1.b,c,d,e, the maxima extracted from the EAP at the different radii, catch the crossing structure. Then, exploiting the angular information at any radius, our EAP-tract method efficiently resolves the crossing region where the ODF-tract fails. Only, few fibers do not follow the right path, whereas all the fibers from ODF-tract follow the wrong path. We see in the next experimental section that our method enables, as well, to recover fibers from other configurations such as U-shape and kissing. We also present EAP-tract results measurements contaminated with Rician noise with SNR=30,20,10 to the measurements (respectively Fig. 2.c,d,e). Nearly all the fibers pass through the crossing area, which shows the robustness of the EAP-tract to noise. On this example, we also want to show the robustness to the choice of the initial radius R_0 used to start the EAP tract algorithm. Hence, we launch the EAP-tract method with five different initial radii, i.e. $R_0 = 5, 10, 15, 20, 25\mu m$. Then we plot in Fig. 4-left the evolution of radii each track follows during the tractography(R_i in Alg. 2). In Fig. 4-left we perceive the crossing region, when all the curves converge, in the notified area (red circle). The radii from all the track converge approximately to the range $[16 - 18\mu m]$. This is not surprising, if we look at figure 1.b,c,d,e, where the whole angular structure appears at radius $18\mu m$. Via this example, we see that our EAP-tract method is robust to the choice of the initial radius.

Phantom data : We also validate our method on the phantom data used in the contest, the "fiber cup" [6] in MICCAI 2009. The ground truth is available and enables to correctly compare tractography algorithms. This phantom contains realistic fibers configurations such as crossing, kissing and bending.

Data pre-processing was allowed for the contest. However, in our experiments, we consider the raw data set. We perform our validation as following : 1) We choose a starting voxel v within the seed proposed for the contest. 2) We launch our algorithm on N_s points taken at random in the voxel v. This step results in N_s

Fig. 2. Tracking on a synthetic crossing region. a,b) are respectively the ODF-tract and EAP-tract in case of noiseless measurements. c,d,e) EAP-tract with measurements contaminated with rician noise (respectively with a SNR=30,20,10).

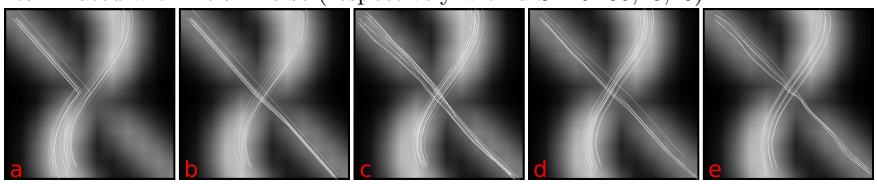

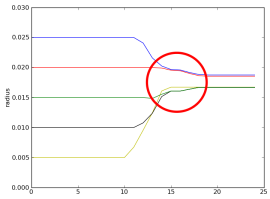

	ODF		EAP	
	F.P.	T.P.	F.P.	T.P.
seed 1	4	0	3	17
seed 8	0	21	0	12
seed 7	17	2	2	13
seed 11	5	1	0	4
seed 14	0	22	0	25
seed 15	11	5	5	12

Fig. 3. Left : Convergence of the radius in the EAP-tract method on synthetic data tractography. **Right** : Quantitative results associated to the phantom tracking.

fiber tracks. 3) Within these N_s fibers, we keep only the fibers with a minimum length ℓ_{min}, and discard the fibers that do not stop outside the phantom. 4) Within the remaining fibers, we count : a) the number of fibers following the ground truth, i.e. the true positive (TP); and b) the number of fibers following another track, i.e. the false positive (FP). We launch the validation with $N_s = 30$, $l_{min} = 20$. We use the same algorithm parameters than in sec. 5. The EAP field is estimated via SHORE method. Fig. 4 shows the fiber tracks for 6 configurations corresponding to several seeds given in the fiber cup: A kissing (Purple fibers, seed 8), a U-shape bundle with high curvature (Blue light fibers, seed 14), and four different crossing configurations (Blue curve, seed 1; green curve, seed 7; yellow curve, seed 11; red curve, seed 15). We also write in Tab. 4-right, the number of true and false positive (respectively TP and FP) for each configuration of the two compared methods (EAP-tract and ODF-tract).

First, we note that the EAP-tract fibers are much in-line with the ground truth than the ODF-tract fibers. The ODF-tract method has difficulties to go through the crossing region whereas the EAP-tract method well resolve these crossing regions. These qualitative remarks are confirmed by quantitative results, while considering the Tab. 4-right. All the fibers involved in crossing bundles (seed 1,7,11,15) have a large number of FP compared to the number of TP using the ODF tract method, whereas most of the fibers from the EAP-tract method are TP. In particular, 90% of the ODF-tract fibers from seed 7 do not follow the right path, whereas only 10% of the EAP-tract fibers from seed 7 do not follow the right path. This improvement of the EAP tract over the ODF tract is huge

Fig. 4. Phantom of the "Fiber cup". a) ODF-tract fibers, b) EAP-tract fibers. On the left we show the ground truth fiber bundles and the spatial position of the seeds.

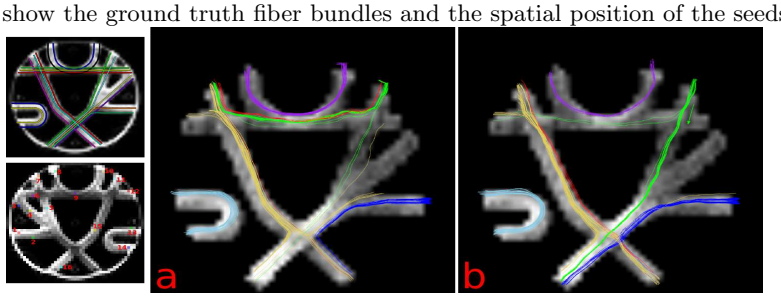

considering the crossing region. In our study we also consider an U-shape (seed 11, light blue curve) and a kissing configuration (seed 8, purple curve). There is no large difference between the two methods for the U-shape configuration. Both efficiently handle high curvature fibers. Considering the kissing case (seed 8, purple curve), there is a small advantage of the ODF-tract method. However, we do not see any FP in both method, which means they can handle kissing fiber configurations efficiently.

To conclude this section, we see that the EAP-tract method efficiently resolve crossing fibers where the ODF-tract fails. Considering other fiber bundle configurations (U-shape and kissing), both methods are equivalent. Hence the advantage of the EAP-tract method lies in its great efficiency to pass trough crossing regions.

Fig. 5. Tractography from the corticospinal fiber bundle (blue), parts of the corpus callosum fiber bundles (red), and the superior longitudinal fasciculus (green). The figure on the right is a zoom on the crossing region between the three bundles.

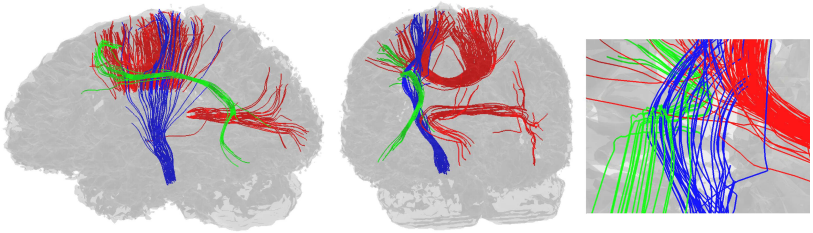

Real data : We present results on a in vivo human cerebral dataset in Fig. 5. This figure shows the corticospinal fiber bundle (CST, in blue), parts of the corpus callosum fiber bundles (CC, in red), and the superior longitudinal fasciculus (green, SLF). These bundles agree with anatomical atlases of the white matter and our EAP-tract method allows a complete distinction between these three

white matter fiber bundles.The zoom (Fig. 5 on the right) shows the crossing region between the CST, the CC and the SLF. Again, the EAP-tract method well resolve this crossing area.

6 Conclusions

In this paper, we proposed and motivated the use of the Ensemble Average Propagator for tractography in dMRI. To the best of our knowledge, it is the first attempt to use the directional information of the EAP at different radii. We illustrated the great potential of the EAP-tract method on synthetic, phantom and real data. These experiments showed that our method is especially efficient to resolve regions where fiber bundles are crossing, and still well handle other fiber bundle configurations such as U-shape and kissing. We also presented numerous examples showing the advantage of the EAP-tract method over the common ODF-tract method. Furthermore, by tracking from seeds in the CC, CST, and SLF, we were able to correctly trace through regions where all three fiber bundles cross.

References

1. Aganj, I., Lenglet, C., Sapiro, G., Yacoub, E., Ugurbil, K., Harel, N.: Reconstruction of the ODF in single and multiple shell q-ball imaging within constant solid angle. Magn. Reson. Med. 64(2), 554566 (2010)
2. Assemlal, H., Tschumperl, D., Brun, L.: Efficient and robust computation of pdf features from diffusion mr signal. Medical Image Analysis 13(5), 715729 (2009)
3. Basser, P.J., Mattiello, J., Le Bihan, D.: Mr diffusion tensor spectroscopy and imaging. Biophysical Journal 66(1), 259267 (1994)
4. Cheng, J., Ghosh, A., Jiang, T., Deriche, R.: Model-free and analytical eap reconstruction via spherical polar fourier diffusion mri. In: MICCAI. vol. 6361, pp. 590–597 (2010)
5. Descoteaux, M., Deriche, R., Knosche, T.R., Anwander, A.: Deterministic and probabilistic tractography based on complex fibre orientation distributions. IEEE Transactions in Medical Imaging 28(2), 269286 (2009)
6. Fillard, P., Descoteaux, M., Goh, A., Gouttard, S., Jeurissen, B., Malcolm, J., Ramirez-Manzanares, A., Reisert, M., Sakaie, K., Tensaouti, F., Yo, T., Mangin, J.F., Poupon, C.: Quantitative analysis of 10 tractography algorithms on a realistic diffusion MR phantom. Neuroimage 56(1), 220234 (2011)
7. Ozarslan, E., Koay, C., Shepherd, T., Blackband, S., Basser, P.: Simple harmonic oscillator based reconstruction and estimation for three-dimensional q-space mri. In: ISMRM. p. 1396. (2009)
8. T. E. J. Behrens, H. Johansen-Berg, S.J.M.F.S.R., Woolrich, M.W.: Probabilistic diffusion tractography with multiple fibre orientations. what can we gain? NeuroImage 34(1), 144155 (2007)
9. Tristan-Vega, A., Westin, S., Aja-Fernandez, S.: Estimation of fiber orientation probability density functions in high angular resolution diffusion imaging. NeuroImage 47(2), 638–650 (2009)
10. Tuch, D.: Q-ball imaging. Magnetic Resonance in Medicine 52(6), 13581372 (2004)